JMEPEG (2011) 20:203–212
DOI: 10.1007/s11665-010-9670-9

1059-9495/$19.00

Tensile Properties and Microstructures of Laser-Formed Ti-6Al-4V

J. Alcisto, A. Enriquez, H. Garcia, S. Hinkson, T. Steelman, E. Silverman, P. Valdovino, H. Gigerenzer, J. Foyos, J. Ogren, J. Dorey, K. Karg, T. McDonald, and O.S. Es-Said

(Submitted December 15, 2009)

The room temperature tensile properties of Ti-6Al-4V alloy prepared under two different processing routes were evaluated and compared. One group of samples was prepared by conventional casting-forging-rolling into flat plates. The other group was prepared by using Triton's Laser Free-Form Fabrication (LF3)™ processes, i.e., a laser was used to melt pre-alloyed powders of the required metallic composition as they were dropped onto a moveable substrate programmed to move in such a manner as to form a solid alloy plate. Five populations of Ti-6Al-4V were evaluated: a standard wrought form, an as-deposited form, a machined as-deposited form, a heat-treated as-deposited form, and a machined as-deposited and heat-treated form. The poorest mechanical properties occurred with the rough surfaces, likely due to existing microcracks and stress concentrations. The LF3™ as-deposited material had mechanical properties comparable to, if not higher than, the mechanical properties of the wrought material. Further evaluations of the laser-formed material for complex spacecraft piece parts were warranted, specifically in regards to improving the surface finish of the materials.

Keywords laser free-form fabrication (LF3), mechanical properties, microstructure, Ti-6Al-4V

1. Introduction

Ti-6Al-4V is the most widely used titanium alloy (Ref 1). It accounts for more than 50% of all titanium usage in the world, with the aerospace industry utilizing more than 80% of this usage. In its wrought form, this alloy accounts for more than 95% of the market (Ref 2, 3). Its applications are mostly in the aircraft industry for jet engine auxiliary parts, for aerospace frames and for chemical processing plants (Ref 1). Ti-6Al-4V alloys are widely used in industrial sectors due to their good stability at high temperature, high specific strength, especially at high operating temperatures, and good corrosion resistance in many corrosive media (Ref 3).

Ti-6Al-4V is an expensive material. Its nominal cost is approximately $59.53 per kg (nominally $27 per lb) (Ref 4). Through conventional means, Ti-6Al-4V components are typically made through casting, forging, and powder metallurgy processes, but Ti-6Al-4V castings are about two to three times the cost of superalloy castings due to the required process conditions. Forging processes cannot easily produce complex shapes, and powder metallurgy processes result in components with lower mechanical properties (Ref 2). Additionally, Ti-6Al-4V is very difficult to weld, increasing the price to produce components by conventional means even further (Ref 2).

An approach based on laser deposition has been developed to overcome this waste of expensive metal. Laser deposition processes differ from traditional forming techniques in the sense that they require no mechanical contact and, therefore, offer the advantage of process flexibility (Ref 5). Laser forming can produce geometries and shapes that are pre-designed out of metallic components with minimal distortion. The inherent advantage of using laser melting techniques is to control both location of the beam and the resulting component microstructure, leading to better service performance of components (Ref 5, 6).

In laser forming, pre-alloyed metallic powder particles are dropped onto a mobile platform (a substrate surface) and are melted while in transit by a laser. Typical commercial laser deposition processes include the Laser Engineering Net Shape (LENS^{tm}) process and AeroMet's Laser Additive Manufacturing (LAM) process. This article introduces a process known as the Laser Free-Form Fabrication (LF3™) process. All three of these techniques are considered laser surface-melting (LSM) processes that allow the user to modify the surface properties of engineering components at selected areas with micron level precision and without distortion. A detailed description of these processes is given in Ref 7-16. Figure 1 demonstrates the LF3™ process.

Since rapid prototype manufacturing was first invented more than 25 years ago, there was demand within industry to make prototypes not just out of plastic/polymer resin materials, but out of more robust materials; even out of the end design material, if possible. At best, the early rapid prototyping parts could be used as patterns to investment cast parts out of the metal alloy of choice, but the ultimate goal remained to direct

J. Alcisto, A. Enriquez, H. Garcia, S. Hinkson, J. Foyos, J. Ogren, J. Dorey, and **O.S. Es-Said**, Mechanical Engineering Department, Loyola Marymount University, One LMU Drive, Los Angeles, CA 90045; **T. Steelman, E. Silverman,** and **P. Valdovino**, Northrop Grumman, Space Technology, One Space Park, Redondo Beach, CA 90278; and **H. Gigerenzer, K. Karg,** and **T. McDonald**, Triton Systems Incorporated, 200 Turnpike Road, Chelmsford, MA 01824. Contact e-mail: oessaid@lmu.edu.

manufacture near-net-shape components using only a CAD file and wire or powder forms of the metal alloy of choice. The evolution of LF3™, LENS™, and other LAM processes from rapid prototyping basically involved the incorporation of higher power lasers and tighter control of the fabrication environment (ambient gases) as well as the development of equipment and techniques to accommodate the processing of metal alloys.

The purpose of this study was to develop an initial database in which the mechanical properties of Ti-6Al-4V prepared by two processing routes could be compared. The goal was to determine if the properties of the laser-formed material, using the LF3™ technique, were sufficiently close to wrought Ti-6Al-4V to allow this material to replace conventionally processed spacecraft hardware. The impetus for the activity was a desire to reduce the manufacturing cost of selected parts of spacecraft hardware.

2. Experimental

In this initial evaluation of the LF3™ process, simple rectangular plates were used as the test materials. The plates were furnished by Triton Systems, Inc. in the form of plates 10 by 20 by 0.2 cm (4 by 8 by 0.08 in.) in the *x*-, *z*-, and *y*-directions, respectively. One such plate is shown schematically in Fig. 2(a). The dotted lines in the figure depict the paths along which the alloy was deposited. The *x*-direction was arbitrarily chosen to be the "parallel" direction or the length, while the *z*-direction was chosen to be the "transverse" direction or the height, and the *y*-direction was the thickness. Figure 2(a) shows schematically the orientations of the tensile samples that were extracted from the plates. The tensile tests were conducted at least in triplicate, and the values quoted later in this article are the averages of the three measured values, Table 1.

The top surface shown in Fig. 2(b) and (c) is an as-deposited surface and, for all the plates, it was rough. These are the surfaces that will be denoted as not machined. The side surfaces of the tensile samples were always machined in the process of making tensile samples.

Triton Systems, Inc. deposited seven plates, which were designated as 1-7, Fig. 3. Some were not machined (1 and 7), others were machined (2-6), some were heat treated (5-7), and others were not (1-4). The deposition conditions and all compositional information regarding the plates are commercially sensitive and therefore are unavailable in detail. These deposition conditions and compositional information include some of the following process parameters and specifications. LF3™ process control involves parameters such as inert chamber gas type and quality (parts per million of oxygen), laser power, laser pulse rate, laser beam focal length and spot size at focus, powder feed rate, traverse speeds, bead overlap and others. The control of the metal alloy powder includes specifications such as alloy composition and oxygen content, porosity levels within particles, particle shape, and particle size. However, all plates were deposited using the same conditions.

Figure 3 depicts the orientations of the tensile samples extracted from the plates. The dotted lines indicate the path of the laser deposit. The *x*-direction indicates the length and the *z*-direction indicates the long transverse direction of the deposited material. Tensile bars designated (*x*) have the deposited layers along the length of the tensile bars, and those designated (*z*) have the layers perpendicular to the tensile bars, Fig. 2(b) and (c). The tensile samples in the *x* and *z* directions were machined from the seven plates and characterized by the number of the plate. For example, 1*x* characterized a tensile bar machined from plate 1 in the *x* direction.

Plates 2 and 3 differ in that the samples in plate 2 were extracted from a section of the plate that was deposited at the beginning of a particular run. In contrast, the samples in plate 3 were taken from the section of the plate that was deposited toward the end of a particular deposition run.

Plates 3 and 4 differ in that one is orthogonal to the other. In other words, plate 4 represents a run in which numerous short

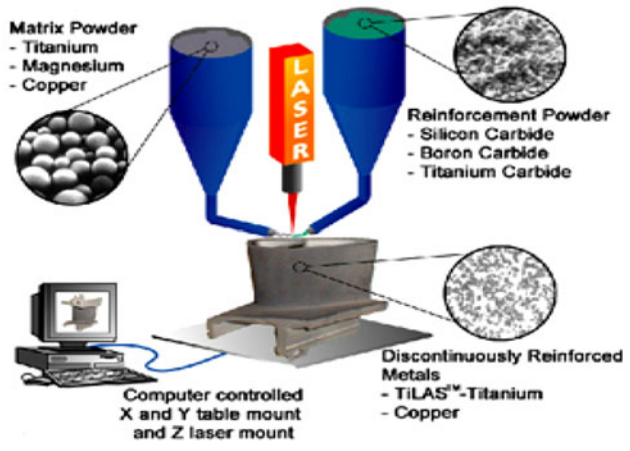

Fig. 1 Schematic view of laser forming

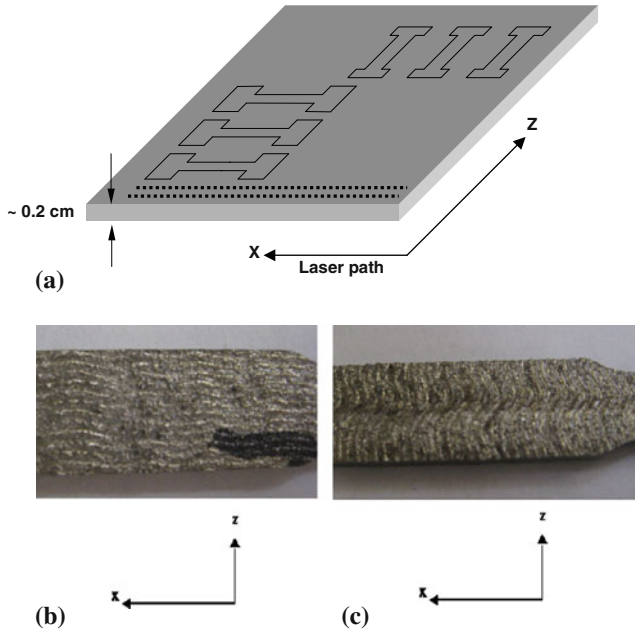

Fig. 2 (a) Schematic view of a laser-formed Ti-6Al-4V plate from which tensile samples were extracted. The *dotted lines* depict the path of metal deposition. The actual plates were approximately 0.2 cm (0.08 in.) thick. (b) As-deposited surface in the *x-direction*. The specimen is 0.9525 cm (0.375 in.) wide. (c) As-deposited surface in the *z-direction*. The specimen is 0.9525 cm (0.375 in.) wide

Table 1 Tensile properties of wrought and laser formed plates

Plate #	ID	Width cm, in.		Thickness, cm/in.		σ_u, ksi/MPa		σ_y, ksi/MPa		% Elong.
Wrought	1a	1.27	0.50	0.24	0.093	153.1	1055.9	139.0	958.6	13.9
	1b	1.29	0.51	0.24	0.093	154.0	1062.1	140.5	969.0	16.7
	1c	1.26	0.49	0.24	0.093	154.0	1062.1	140.1	966.2	12.4
	1d	1.26	0.49	0.24	0.093	155.0	1069.0	140.9	971.7	13.9
	1e	1.26	0.49	0.24	0.093	154.5	1065.5	139.8	964.1	12.3
	Avg					154.1	1062.9	140.1	965.9	13.8
1 As-deposited not machined	1x1	0.67	0.26	0.25	0.1	132.4	913.1	129.7	894.5	6.0
	1x2(a)	0.65	0.25	0.25	0.1	133.9	923.4	131.3	905.5	6.0
	1x3	0.65	0.25	0.25	0.1	130.8	902.1	127.7	880.7	6.3
	1x4	0.64	0.25	0.25	0.1	131.2	904.8	128.8	888.3	7.2
	Avg					132.1	910.9	129.4	892.2	6.4
	1z1	0.66	0.26	0.25	0.1	119.0	820.7	75.7	522.1	1.5
	1z2	0.64	0.25	0.25	0.1	114.9	792.4	n/a	n/a	2.0
	1z3	0.65	0.25	0.25	0.1	110.4	761.4	n/a	n/a	1.4
	1z4(a)	0.65	0.25	0.25	0.1	118.0	813.8	75.8	522.8	2.0
	Avg					115.6	797.1	75.8	522.4	1.7
2 As-deposited machined	2x1	0.69	0.27	All thickness		156.0	1075.9	136.4	940.7	n/a
	2x2	0.64	0.25	were within		155.6	1073.1	139.1	959.3	7.7
	2x3(a)	0.68	0.27	0.15-0.2 cm		152.2	1049.7	137.0	944.8	5.9
	2x4(b)	0.69	0.27	(0.06-0.08 in.)		149.8	1033.1	n/a	n/a	n/a
	Avg					153.4	1057.9	137.5	948.0	6.8
	2z1	0.64	0.25	All thickness		145.5	1003.4	n/a	n/a	3.5
	2z2(a)	0.69	0.27	were within		149.4	1030.3	137.3	946.9	3.8
	2z3	0.68	0.27	0.15-0.2 cm		142.7	984.1	135.7	935.9	n/a
	2z4	0.68	0.27	(0.06-0.08 in.)		148.7	1025.5	134.9	930.3	5.7
	Avg					146.6	1010.9	136.0	937.7	4.3
3 As-deposited machined	3x1	0.64	0.25	All thickness		160.8	1109.0	149.2	1029.0	4.6
	3x2	0.64	0.25	were within		156.2	1077.2	142.5	982.8	5.7
	3x3	0.64	0.25	0.15-0.2 cm		156.1	1076.6	142.3	981.4	4.4
	3x4	0.64	0.25	(0.06-0.08 in.)		155.7	1073.8	144.4	995.9	n/a
	3x5(a)	0.64	0.25			156.3	1077.9	143.3	988.3	4.5
	Avg					157.0	1082.9	144.3	995.4	4.8
	3z2(a)	0.64	0.25	All thickness		148.5	1024.2	136.9	944.1	3.5
	3z3	0.65	0.25	were within		149.6	1031.8	141.0	972.4	4.0
	3z4	0.64	0.25	0.15-0.2 cm		149.7	1032.5	138.0	951.7	3.9
	3z5	0.64	0.25	(0.06-0.08 in.)		150.9	1040.7	138.8	957.2	4.6
	Avg					149.7	1032.4	138.7	956.4	4.0
4 As-deposited machined	4x1	0.64	0.25	All thickness		157.2	1084.1	145.6	1004.1	5.0
	4x2	0.64	0.25	were within		153.2	1056.6	141.9	978.6	5.4
	4x3	0.64	0.25	0.15-0.2 cm		152.7	1053.10	142.7	984.1	n/a
	4x4	0.64	0.25	(0.06-0.08 in.)		155.1	1069.7	144.1	993.8	5.8
	4x5	0.64	0.25			156.2	1077.2	146.5	1010.3	n/a
	Avg					154.9	1068.1	144.2	994.2	5.4
	4z1(b)	0.64	0.25	All thickness		150.5	1037.9	143.1	986.9	n/a
	4z2(a)	0.65	0.25	were within		152.2	1049.7	138.5	955.2	3.5
	4z3(b)	0.64	0.25	0.15-0.2 cm		147.7	1018.6	140.5	969.0	n/a
	4z4(b)	0.64	0.25	(0.06-0.08 in.)		148.8	1026.2	137.6	949.0	3.3
	4z5	0.64	0.25			150.4	1037.2	141.0	972.4	2.4
	Avg					151.3	1043.5	139.8	963.8	3.0
5 Heat-treated machined(c)	5x1	0.60	0.23	All thickness		140.0	965.5	125.6	866.2	n/a
	5x2(b)	0.59	0.23	were within		137.5	948.3	n/a	n/a	n/a
	5x3(a)	0.64	0.25	0.15-0.2 cm		138.3	953.8	123.9	854.5	14.6
	5x4	0.63	0.25	(0.06-0.08 in.)		136.9	944.1	123.0	848.3	10.6
	5x5	0.63	0.25			131.5	906.9	n/a	n/a	10.5
	Avg					136.8	943.7	124.2	856.3	11.9
	5z1	0.64	0.25	All thickness		135.5	934.5	n/a	n/a	7.0
	5z2(a)	0.63	0.25	were within		136.2	939.3	n/a	n/a	8.5
	5z3	0.62	0.24	0.15-0.2 cm		136.2	939.3	n/a	n/a	8.0
	5z4	0.64	0.25	(0.06-0.08 in.)		139.6	962.8	122.8	846.9	8.1
	5z5	0.63	0.25			140.3	967.6	123.0	848.3	7.3
	Avg					137.6	948.7	122.9	847.6	7.8

Table 1 Continued

Plate #	ID	Width cm, in.		Thickness, cm/in.	σ_u, ksi/MPa		σ_y, ksi/MPa		% Elong.
6 Heat-treated machined	6x1	0.64	0.25	All thickness	139.4	961.4	128.9	889.0	11.0
	6x2	0.63	0.25	were within	139.5	962.1	124.6	859.3	11.7
	6x3	0.64	0.25	0.15-0.2 cm	139.8	964.1	124.4	857.9	11.7
	6x4	0.62	0.24	(0.06-	138.8	957.2	123.9	854.5	11.4
	6x5	0.64	0.25	0.08 in.)	140.2	966.9	122.2	842.8	12.6
	Avg				139.5	962.3	124.8	860.7	11.7
	6z1	0.64	0.25	All thickness	136.2	939.3	121.9	840.7	12.6
	6z2	0.64	0.25	were within	134.9	930.3	119.2	822.1	12.6
	6z3	0.64	0.25	0.15-0.2 cm	136.8	943.4	117.7	811.7	11.7
	6z4	0.63	0.25	(0.06-	135.0	931.0	119.5	824.1	10.8
	6z5	0.63	0.25	0.08 in.)	135.5	934.5	118.4	816.6	10.8
	Avg				135.7	935.7	119.3	823.0	11.7
7 Heat-treated no machine	7x1	0.64	0.25	0.25 0.1	103.8	715.9	89.9	620.0	5.2
	7x2	0.63	0.25	0.25 0.1	111.0	765.5	102.8	708.3	3.8
	7x3(a)	0.64	0.25	0.25 0.1	110.5	762.1	100.6	693.8	3.3
	7x4	0.64	0.25	0.25 0.1	109.0	751.7	100.2	691.0	6.8
	7x5	0.65	0.25	0.25 0.1	109.2	753.1	100.5	693.1	n/a
	Avg				108.7	749.7	98.8	681.2	4.8
	7z1	0.64	0.25	All thick-	101.5	700.0	n/a	n/a	n/a
	7z2	0.63	0.25	nesses were	105.2	725.5	94.7	653.1	4.6
	7z3	0.65	0.25	within 0.15-	105.3	726.2	92.1	635.2	3.8
	7z4	0.64	0.25	0.2 cm (0.06-	103.8	715.9	90.0	620.7	2.9
	7z5	0.64	0.25	0.08 in.)	n/a	n/a	92.5	637.9	2.3
	Avg				104.0	716.9	92.3	636.7	3.4

(a) Samples used for metallography
(b) Sample broke *then* computer beeped; corresponding values not included in average
(c) Surface mill both sides

(10 cm) lines were deposited while, in contrast, plate 3 represents a case of fewer but longer deposition lines.

Heat treating of the as-deposited material was at 980 °C for one hour followed by furnace cool-down in vacuum. This thermal treatment is close to the solutionizing temperature, 900-970 °C for this alloy (Ref 17). Plates 5-7 were heat treated, Fig. 3. The transus temperature for Ti-6Al-4V is 1000 °C, so the heat treating at 980 °C did not result in a full beta anneal.

Tensile testing was performed on an Instron 4505 unit Model 4500 Control Module. Testing was at ambient temperature (23 °C) and in laboratory air. The sample gauge length was 2.54 cm (1 in.) and the widths of the samples are presented in Table 1. An extensometer was used during the tensile tests and the strain rate was 0.127 cm/min (0.05 in./min).

After tensile testing, the grip area of the coupons was used for metallographic examination. Both longitudinal and transverse samples were mounted in a cold setting plastic/polymer and were ground, polished, and etched (Keller's reagent) according to standard practice (Ref 18). No isostatic pressing was performed on any of the test materials.

3. Results

The tensile data are summarized in Fig. 4 and 5 and are compiled in Table 1 for all the samples. Yield and tensile strength bar charts are presented in Fig. 4 and 5; elongation values are in Fig. 6. In every figure, data for the wrought material are included for comparison. The tensile values obtained for the wrought material, 966 MPa (140 ksi) in yield strength, are consistent with it being beta-annealed at 865 °C (Ref 1).

The strengths of the laser deposited not machined and heat-treated material (plates 1, 5-7) were generally less than that of the wrought material. An important exception is the as-deposited machined samples (plates 2-4). This material is stronger than the wrought material; however, its elongation is less (~5% compared to ~14%).

Optical micrographs of the wrought and the as-deposited laser formed samples (with and without heat treatment) are shown in Fig. 7-10. SEM micrographs of the fracture surface of the tensile bars are shown in Fig. 11. The microstructure of as-deposited laser formed material is shown in Fig. 8 and reflect the acicular α-β that is frequently found in such quenched structures.

The heat-treated-laser-formed microstructure is shown in Fig. 10 and shows all the features of Ti-6Al-4V that had been heat treated in the two-phase alpha-beta region of the Ti-Al phase diagram. The microstructure consists of platelets of the alpha phase (light color) in a matrix of an intimate mixture of alpha and transformed beta phase (Ref 19, 20).

Low magnification optical images shown in Fig. 2(b) and (c) show the rough top surface of the depositions. In Fig. 11(a), the fractured surface of a tensile sample from the wrought Ti-6Al-4V indicates ductile fracture with equiaxed dimples. Microvoid coalescence indicative of ductile fracture is shown and the percent elongation is 13.8%, as shown in Table 1.

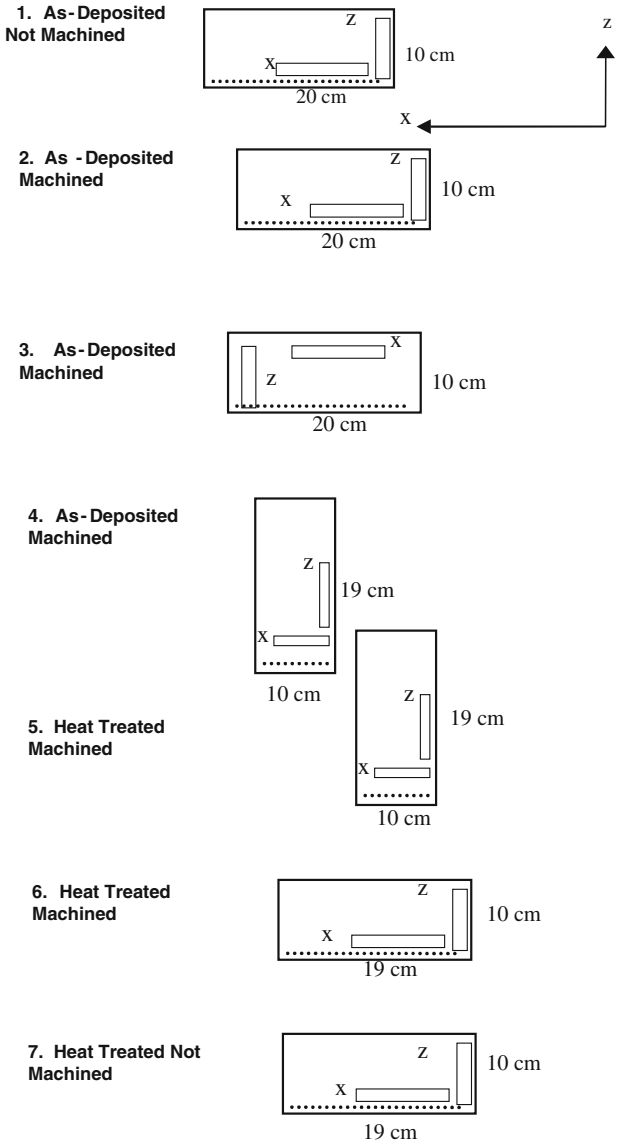

Fig. 3 Schematic views of the orientations of the tensile samples. This figure is intended to display the nomenclature used in this article

In Fig. 11(b) the top surface of an as-deposited laser formed sample is shown. The fractured surface is shown in Fig. 11(c) and (d). The fracture is ductile away from the pores, but these pores accelerate the fracture and lower the ductility. Figure 11(c) also appears to show delineation of prior powder particle boundaries on the fracture surface, to an extent that the responsible features likely participated in the fracture process and the development of properties. Figure 11(e) shows the fractured surface of a laser formed, machined, and heat-treated sample with equiaxed dimples and ductile fracture.

The as-deposited surface, shown in Fig. 11(b), is characterized by abundant splatter droplets, about 100 microns in diameter, and relatively large and deep crevices. The high points on the surface are the characteristic points measured when micrometer measurements were made of the dimensions of the samples when stress values were calculated from tensile loads. The micrometer-measured dimensions do not, in reality, represent the dimensions of the bulk of the stressed material, and, as a consequence, the dimensions used for the cross-sectional areas were a little bit large, and the calculated stress values were slightly smaller than the true values.

4. Discussion

4.1 Effects of Laser Forming and Heat Treatment

The tensile and yield strengths of the wrought Ti-6Al-4V alloy were 1062.9 MPa (154.1 ksi) and 965.9 MPa (140.1 ksi), respectively. The percent elongation was 13.8, from Fig. 4, 7, and Table 1. These values are in accord with the SAE-AMS-T-9046 specifications (Ref 20). The microstructure, which is shown in Fig. 7(a) and (b), consist of a mixture of α and lean refined β phases, which inhibits dislocation slip. The mode of fracture however is ductile, Fig. 11(a). The tensile and yield strengths of the as-deposited non-machined plate 1 samples were 910.9 MPa (132.1 ksi) and 892 MPa (129.4 ksi), respectively. This is a 7-14% reduction in strength as compared to the wrought material. The percent elongation was 6.4, which is 53% lower than that of the wrought material.

The optical micrographs, Fig. 8(a) and (b), reveal numerous microcracks and voids throughout the microstructure, which are stress concentration factors. The microstructure consists of columnar prior-beta grains elongated in the solidification (build) direction; within it is a fine Widmanstatten (basket weave) platelet alpha, which indicates a relatively rapid cooling after solidification (Ref 16). The as-deposited "not machined" rough surfaces, Fig. 2(b) and (c) were responsible for the lack of fusion, interlayer porosity, and the weak strengths and ductility. Figure 11(b)-(d) reveals the mixed mode of brittle/ductile fracture of the as-deposited—"not machined" samples due to excessive voids.

The tensile and yield strengths of the as-deposited machined plates 2-4 were similar to the wrought material strength values. The inclusion of plates 3 and 4 will be discussed in the next section. The tensile and yield strengths of plate 2 are 1057.9 MPa (153.4 ksi) and 948.3 MPa (137.5 ksi), respectively, which is less than 2% differences as compared to the wrought values. The percent elongation is 6.8, which is 50% of the value of the wrought material. The microstructure shown in Fig. 9 reveals a similar microstructure of acicular alpha-beta like that of plate 1 but with less microcracks and pores which explains the improved ductility and strength as compared to those of plate 1, i.e., "not machined."

The mechanical strengths and ductility values of the heat-treated plates 5-7 are summarized in Fig. 4-6. The inclusion of plate 6 will be discussed in the next section. Plates 5-7 were heat treated at 980 °C for one hour followed by furnace cool in vacuum. The tensile and yield strengths of plate 5 were 943.7 MPa (136.8 ksi) and 856.3 MPa (124.2 ksi), respectively, which is 10-11% reduction in strength as compared to the wrought material. The percent elongation was 11.9%, which is 14% lower than that of the wrought material. The microstructure of the heat-treated machined plate showed columnar beta grains with coarser Widmanstatten alpha and most of the porosity was healed, Fig. 10 and 11(e) (Ref 16).

In plate 7, no machining was performed. This was translated to the weak values of strength and ductility. The tensile and

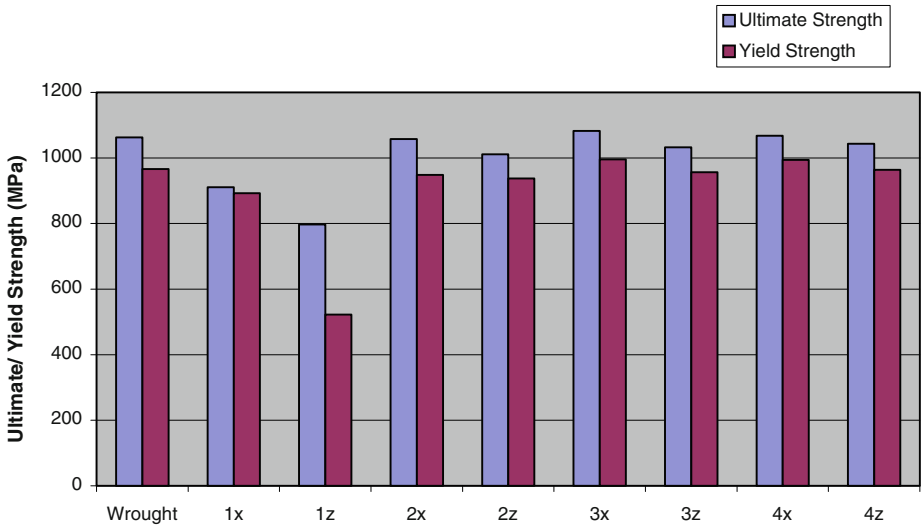

Fig. 4 Tensile values of laser-formed non-heat-treated Ti-6Al-4V. Values for wrought alloy are included for comparison

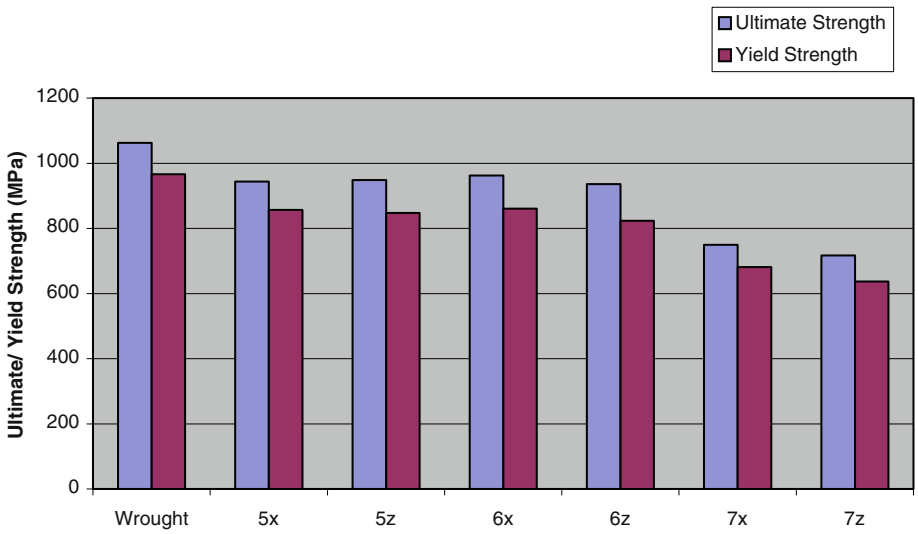

Fig. 5 Tensile values of laser formed heat-treated Ti-6Al-4V. Values for wrought alloy are included for comparison

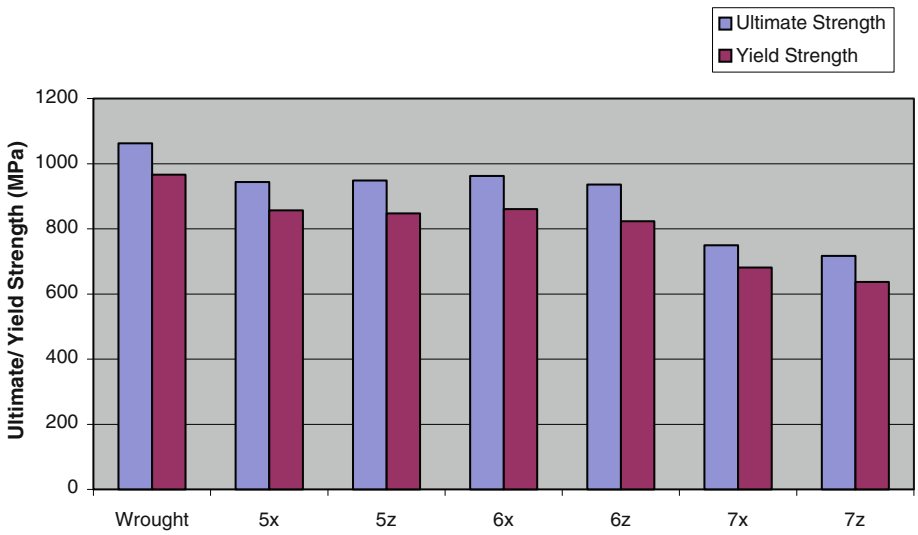

Fig. 6 Elongation values for laser-formed Ti-6Al-4V

yield strengths of plate 7 were 749.7 MPa (108.7 ksi) and 681.2 MPa (98.8 ksi), respectively. These values were around 30% lower than those of the wrought material and 20% lower than those of the heat-treated and machined plate 5. The percent elongation was 4.8, which is 65% of the value of the wrought material and 60% of the value of plate 5. The inclusion of plates 1 and 7 indicates the criticality of removing rough surfaces by machining of the final parts.

The effect of heat-treating the laser formed plates was the transformation of the acicular alpha-beta microstructure, Fig. 9 to a columnar beta grains and coarser Widmanstatten alpha grains and minimum porosity, Fig. 10. This transformation was responsible for around 10-12% decrease in strength and more than doubling of the percent elongation values, as compared to the non-heat-treated samples, Fig. 4-6. The mechanical strength values of plates 3 and 4 were slightly higher than those of the wrought material, however, the percent elongation was much lower, Fig. 4 and 6.

4.2 Effect of Location of Tensile Bars on the Mechanical Properties

In Fig. 3, plates 2 and 3 differ in that the tensile bars in plate 2 were extracted from a section of the plate that was deposited at the beginning of a particular run while the tensile bars in plate 3 were taken from the section of the plate that was deposited toward the end of a particular run. Both plates 2 and 3 are machined and are not heat-treated, Fig. 4. The tensile strengths are similar, which indicates that laser forming process, produces uniform mechanical properties.

Plates 3 and 4 (non-heat treated and machined) and plates 5 and 6 (heat treated and machined) differ in that one is orthogonal to the other, plate 4 (and plate 5) represents a run in

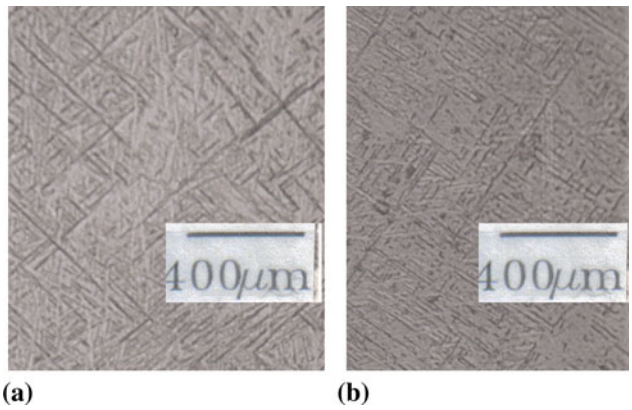

Fig. 7 Long (a) and rolling (b) direction views of the wrought Ti-6Al-4V microstructure after being annealed (beta-aged) at 865 °C

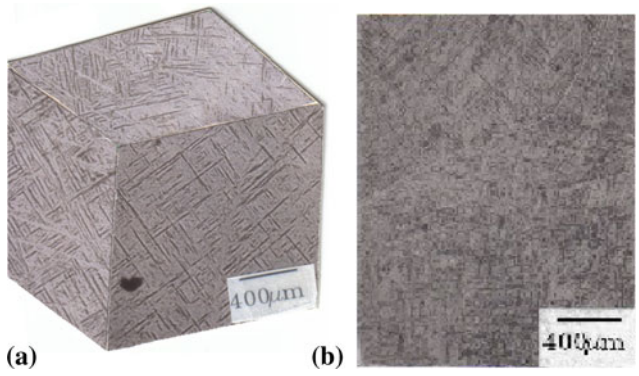

Fig. 8 (a) An isometric view of the microstructure of the as-deposited sample. (b) A longitudinal view of the microstructure of the as-deposited sample

Fig. 9 An isometric view of the microstructure of an as-deposited machined sample

Fig. 10 An isometric view of the microstructure of an as-deposited, machined, and heat-treated sample. The sample was heat treated at 980 °C for one hour

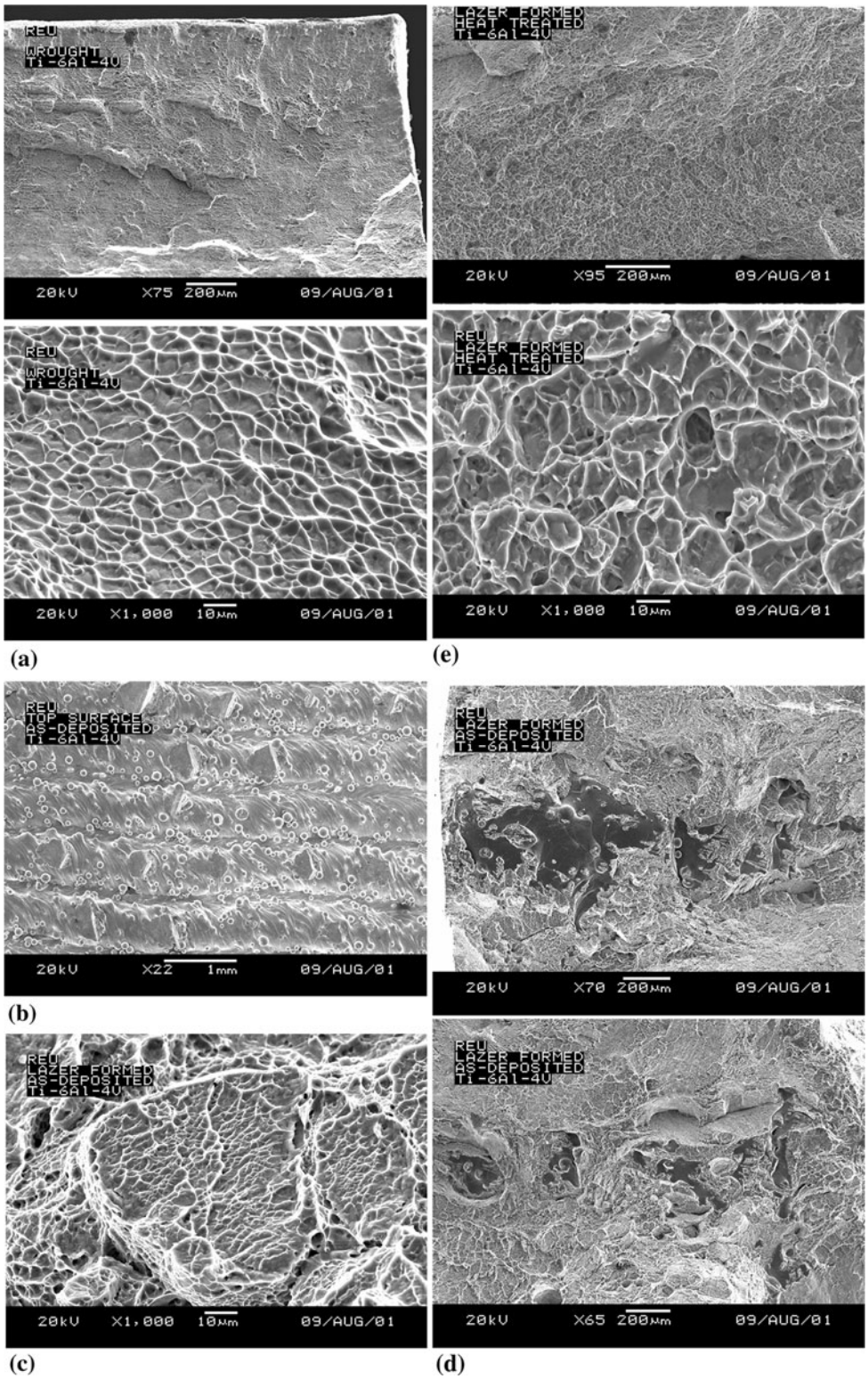

Fig. 11 (a) A scanning electron microscope view of the fractured surface of a tensile specimen of the wrought Ti-6Al-4V. (b) A scanning electron microscope view of the top as-deposited surface. Splatter is seen everywhere. (c) A scanning electron microscope view of the fractured surface of a tensile sample of an as-deposited laser formed sample, high magnification. (d) A scanning electron microscope view of the fractured surface of a tensile sample of an as-deposited laser formed sample, low magnification. (e) A scanning electron microscope view of the fractured surface of a tensile sample of an as-deposited/heat-treated laser formed sample

which numerous short (10 cm) lines were deposited while in contrast, plate 3 (and plate 6) represents a case of fewer but longer deposition lines. The tensile properties between plates 3 and 4 on one hand and plates 5 and 6 on the other hand confirm the homogeneity of properties in different locations of a laser formed product.

Table 2 Anisotropic values of tensile strengths

Plate	Anisotropy in tensile strength, %	Anisotropy in yield strength, %	Average percent elongation in *x*-direction	Average percent elongation in *z*-direction
1	12.5	41.4	6.4	1.7
2	4.4	1.1	6.8	4.3
3	4.7	3.9	4.8	4
4	2.3	3.1	5.4	3.0
5	−0.6	1.1	11.9	7.8
6	2.7	4.4	11.7	11.7
7	4.3	6.7	4.8	3.4

In all laser formed plates 1-7, Fig. 4-6 and Table 1, tensile bars tested in the *x*-direction had better tensile properties as compared to those tested in the *z*-direction. Anisotropy will be defined as:

$$\frac{\sigma_x - \sigma_z}{\sigma_x} * 100\% \quad \text{(Eq 1)}$$

where σ is the tensile or yield strengths and σ_x and σ_z denote strengths at *x* or *z* directions. The anisotropy is shown in Table 2 for each plate. The anisotropic behavior was very significant in plate 1. The tensile strength in the *x* direction is 910.9 MPa (132.1 ksi) and in the *z* direction is 797.1 MPa (115.6 ksi) with a 12.5% anisotropy. The yield strength in the *x* direction is 892.2 MPa (129.4 ksi) and in the *z* direction is 522.4 MPa (75.8 ksi) with a 41.4% anisotropy. Plates 2-7 had less than 5% anisotropy except for the yield strengths in plate 7, 6.7% anisotropy, Table 2.

These results can be related to the work of Es-Said et al. (Ref 21). In this work, rapid prototype ABS (Acrylonitrile-Butadienre-Styrene) P400 samples were deposited in a 0° degree orientation, where the layers were deposited along the length of the tensile samples like the *x* direction tensile bars of this study, Fig. 2(b). They (Ref 21) also deposited the polymer samples in a 90° orientation, where the layers were at a 90° angle to the length of the tensile samples similar to the *z* direction tensile bars of this study, Fig. 2(c). The 0° degree orientation in the polymer rapid prototype study (Ref 21) not only was significantly higher in strength as compared to the 90° orientation, but was also significantly higher in toughness. The same is true in the *x* and *z* direction of plate 1 of this study, since the percent elongation is 6.4% for the *x* direction and 1.7% in the *z* direction. Es-Said et al. (Ref 21) related this behavior to weak interfaces in 2D layered materials (Ref 19). Weak interfacial layers at 0° orientation (*x* direction in this study) that are perpendicular to the crack front will absorb high amounts of energy due to interface delamination (Ref 19, 22). The delamination will blunt the crack tip, reduce the stresses ahead of the crack and cause higher amounts of energy to be absorbed for crack propagation. The weak interfaces are parallel to the crack front at the 90° orientation (*z* direction in this study) and will provide an easy path for crack propagation and cause small amounts of energy to be absorbed.

The low strength values of the *z* direction as compared to the *x*-direction in plate 1 confirm the hypothesis that the strength anisotropy is affected by the directional processing of the 2D laminates or the preferred orientation of weak interfaces and interlayer porosity (Ref 22).

The low strength values of both *x* and *z* direction in plate 1 compared to the strength values of all other plates 2-7 can be explained by the presence of interlayer porosity (Fig. 8a, b, 11b-d). Interlayer porosity reduces the load-bearing area across the layers and hence provides an easy fracture path (Ref 19). It was clear that machining and or heat-treating had the effect of significantly reducing the porosity and anisotropy in all other plates.

5. Conclusions

1. Laser-formed Ti-6Al-4V materials have been tested for mechanical properties, and have been found to exhibit mechanical strengths comparable, and in some tests, superior to the conventional wrought alloy. The percent elongation however was consistently lower than that of the wrought material.
2. The as-deposited laser formed surfaces were rough and showed crack initiation sites due to porosity. This was a cause also of anisotropy in the mechanical strength.
3. The tensile properties were uniform at all locations of a laser formed plate.
4. The tensile properties of the laser-formed material were isotropic within the plane of the deposited material when machined or heat treated or both.

Acknowledgments

The authors wish to acknowledge the financial support for this project from the National Science Foundation, Grant No. EEC 0097863. They also wish to thank Ms. Jaisey Simard and Mr. Roman Silva for preparing the manuscript.

References

1. M. Donachie, *Titanium, A Technical Guide*, 2nd ed., ASM International, Materials Park, OH 44073, 2000, p 5–8
2. H.R. Salimijazi, T.W. Coyle, and J. Mostaghimi, Vacuum Plasma Spraying: A New Concept for Manufacturing Ti-6Al-4V Structures, *JOM*, September 2006, p 50–56
3. R. Boyer, G. Welsch, and E.W. Collings, Ed., *Materials Properties Handbook: Titanium Alloys*, ASM International, Materials Park, OH, 1998, p 3–31
4. R. Witt, Inside Sales Manager, Service Steels Aerospace, (P) 800.624.8073, http://www.ssa-corp.com/quotation.asp, August 24, 2009
5. K.G. Watkins, S.P. Edwardson, J. Magee, G. Dearden, and P. French, Laser Forming of Aerospace Alloys, *Aerospace Manufacturing Technology Conference (AMTC)*, SAE, 2001, p 1–7
6. B.V. Krishna and A. Bandyopadhyay, Surface Modification of AISI 410 Stainless Steel Using Laser Engineered Net Shaping (LENS^{tm}), *Mater. Des.*, 2008, doi:10.1016/j.matdes.2008.08.003
7. R. Banerjee et al., Microstructural Evolution in Laser Deposited Compositionally Graded Alpha/Beta Titanium-Vanadium Alloys, *Acta Mater.*, 2003, **51**, p 3277–3292
8. D.M. Keicher and W.D. Miller, LENS Moves Beyond RP to Direct Fabrication, *Metal Powder Rep.*, 1998, **53**, p 26–28
9. B. Cleveland, Rapid Manufacturing Technologies, *Adv. Mater. Process.*, 2001, **159**(5), p 32
10. J. Brooks, C. Robino, T. Headley, S. Goods, and M. Griffith, *Microstructure and Property Optimization of LENS Deposited H13 Tool Steel. Solid Freeform Fabrication Proc*, University of Texas, Austin, 1999
11. P.L. Blackwell and A. Wisbey, Laser-aided Manufacturing Technologies; Their Application to the Near-Net Shape Forming of a

High-Strength Titanium Alloy, *J. Mater. Process. Technol.*, 2005, **170**, p 268–276
12. K.P. Cooper, Building Components by Laser-Additive Processing, *JOM*, 2001, **53**(9), p 29
13. P.A. Kobryn and S.L. Semiatin, *Mechanical Properties of Laser-Deposited Ti-6Al-4V*, AFRL/MLLMP, p 179–186
14. S.M. Kelly, S.L. Kampe, and C.R. Crowe, Microstructural Study of Laser Formed Ti-6Al-4V, *Solid Freeform and Additive Fabrication Symposium*, Vol. 625, 2000, p 3–8
15. P.A. Kobryn and S.L. Semiatin, The Laser Additive Manufacture of Ti-6Al-4V, *JOM*, 2001, **53**, p 40–42
16. S.L. Semiatirn et al., Plastic Flow and Microstructure Evolution during Thermomechanical Processing of Laser-Deposited Ti-6Al-4V Performs, *Met. Mater. Trans. A*, 2001, **32A**, p 1802
17. MIL Standard H-812008, Jan 13, 1991
18. G. Kehl, *Principles of Metallographic Laboratory Practice*, 3rd ed., McGraw-Hill Book Publishing Company, New York, 1949
19. S.A. Salpekar, I.S. Raju, and T.K. O'Brien, Strain-Energy Release Rate Analysis of Delamination in a Tapered Laminate Subjected to Tension Load, *J. Compos. Mater.*, 1991, **25**, p 118
20. SAE-AMS-T-9046, "Titanium and Titanium Alloy, Sheet, Strip, and Plate," 17 September 1999
21. O.S. Es-Said, J. Foyos, R. Noorani, M. Mendelson, and B. Pregger, Effect of Layer Orientation on Mechanical Properties of Rapid Prototyped Samples, *Mater. Manuf. Process.*, 2000, **15**(1), p 112
22. A.S. Brown, *Rapid Prototyping: Parts Without Tools*, Aerospace America, 1991, p 18